Electronic Supplementary Information (ESI)

High-performance "sweeper" for toxic cationic herbicides: an anionic metal–organic framework with tetrapodal cage

Yan-Yuan Jia[a], Ying-Hui Zhang[b], Jian Xu[b], Rui Feng[b], Ming-Shi Zhang[a] and Xian-He Bu[a,b]*

[a] Department of Chemistry, Collaborative Innovation Center of Chemical Science and Engineering (Tianjin), Nankai University, Tianjin 300071, China.

[b] School of Materials Science and Engineering, TKL of Metal- and Molecule-Based Material Chemistry, Nankai University, Tianjin 300071, China.

* Corresponding author. E-mail: buxh@nankai.edu.cn

S1. Materials and methods

All the Chemicals were purchased from commercial sources and used without further purification. Powder X-ray diffraction (PXRD) spectra were recorded on a Rigaku D/Max-2500 diffractometer at 40 kV and 100 mA for a Cu-target tube and a graphite monochromator. Thermogravimetric analyses (TGA) were carried out on a Rigaku standard TGDTA analyzer under N_2 with a heating rate of 10 °C min^{-1}, using an empty Al_2O_3 crucible as reference. Simulation of the PXRD pattern was carried out based on the single-crystal data by diffractioncrystal module of the Mercury (Hg) program version 1.4.2 available free of charge via the Internet at http://www.iucr.org. UV-Visible absorption spectral measurements were carried out on a U-3010 Spectrophotometer. The residues of MV and DQ upon adsorption in alcohol solution was determined by LC-MS/MS analysis on OA_SPE Waters Xevo TQ_S instrument. All the pesticides solution were prepared in HDPE (High Density Polyethylene) bottles.

S2. Crystal Structure Determination

All diffraction data were collected on a Rigaku SCX-mini diffractometer at 293(2) K with Mo-Kα radiation (λ = 0.71073 Å) by ω scan mode. The structures were solved by direct methods using the SHELXS program of the SHELXTL package and refined with SHELXL.[S1] The disordered solvent molecules and $[(CH_3CH_2)_2NH_2]^+$ in NKU-**101** are removed by SQUEEZE as implemented in PLATON[S2] and the results were appended in the CIF files.

S3. Synthesis of NKU-101

NKU-**101** was synthesized by the solvothermal reaction of H_3BTC (84.01 mg, 0.4 mmol), H_2PyC (22.41 mg, 0.2 mmol) and $Zn(NO_3)_2{\cdot}6H_2O$ (208.24 mg, 0.7 mmol) in N,N-Diethylformamide (DEF, 10mL) at 140°C for 72 hours to give block-shaped colorless crystals (Yield: ~60% based on H_2PyC).

S4. Sorption Measurements

Gas adsorption measurements were performed using an ASAP 2020 M gas adsorption analyzer. Before the measurements, the sample of NKU-**101** was soaked in ethanol for 2 days, and then filtrated and activated under high vacuum (less than 10^{-5} Torr) at 120 °C. About 205 mg activated sample were used for gas sorption measurements.

For NKU-**101**, the N_2 sorption isotherms at 77 K were collected in a liquid nitrogen bath, at 273 K in an ice water mixture bath and at 298 K in an electric heating jacket. The H_2 sorption isotherms were at 77 K collected in a liquid nitrogen bath and at 87 K in a liquid argon bath. The CO_2 and CH_4 sorption isotherms at 273 K and 298 K were collected in the same conditions with that of N_2 sorption under that same temperatures.

In order to examine the permanent porosity of NKU-**101**, the gas adsorption experiments were performed. The as-synthesized NKU-**101** sample exhibits high thermal stability (Fig. S6) and crystal purity demonstrated by good agreement of experimental powder X-ray diffraction (PXRD) pattern with the simulated one (Fig. S7). The N_2 sorption isotherm at 77 K of activated sample demonstrates typical Type I characteristic (Fig. S8), with a Brunauer–Emmett–Teller (BET) and Langmuir surface area of 847 $m^2 \cdot g^{-1}$ and 1114 $m^2 \cdot g^{-1}$, respectively. The pore distribution analysis by H-K (Horvath–Kawazoe) method shows a main distribution in the range of 0.8-1.2 nm (Fig. S8 (Inset)). Subsequently, the H_2 adsorption at 1 atm for NKU-**101** was carried out (Fig. S9), which reveals an average H_2 adsorption capacity of 134.68 $cm^3 \cdot g^{-1}$ at 77 K and 96.16 $cm^3 \cdot g^{-1}$ at 87 K, respectively. Furthermore, CO_2, CH_4, and N_2 adsorption of NKU-**101** were also investigated at 273 K and 298 K (Fig. S10-S11). The CO_2 uptakes at 1 atm are 65.29 $cm^3 \cdot g^{-1}$ at 273 K and 37.03 $cm^3 \cdot g^{-1}$ at 298 K, the adsorption quantity of CH_4 at 1 atm reach 17.83 and 10.49 $cm^3 \cdot g^{-1}$ at 273K and 298 K, while that of N_2 are only 5.09 and 3.03 $cm^3 \cdot g^{-1}$ recorded at 273 K and 298 K, respectively. The adsorption enthalpies (Q_{st}) of H_2, CO_2 and CH_4 are calculated by Virial method (Fig. S12-S14), with the values of 6.41, 23.10 and 18.50 $kJ \cdot mol^{-1}$ at zero loading, respectively. Notably, the PXRD pattern of the sample after gas adsorption still exhibits good agreement with the simulated one, indicating the high stability of NKU-**101** framework sufficient for surviving after gas adsorption and desorption (Fig. S7).

S5. Residual Measurements

The residues of MV and DQ in alcohol solution was determined through LC-MS/MS analysis on OA_SPE Waters Xevo TQ_S instrument equipped with a BEH C18 column (50*2.1 mm, 1.7 μm, Waters), using 5 mmol·L^{-1} ammonium acetate buffered solution mixed with 0.2% formic acid (V/V) as mobile phase A and acetonitrile (HPLC pure) as mobile phase B.

At first, an experimental standard curve of concentration-peak areas of LC-MS/MS in alcohol solution was depicted for DQ, and then the residues of DQ upon adsorption was deduced by comparing its corresponding experimental peak area of LC-MS/MS with standard curve.

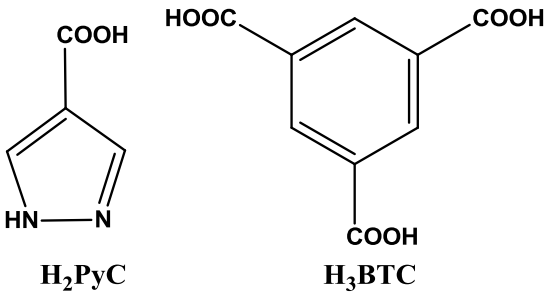

Scheme S1 The structures of H_2PyC and H_3BTC (H_2PyC = 4-pyrazolecarboxylic acid, H_3BTC = 1,3,5-benzenetricarboxylic acid).

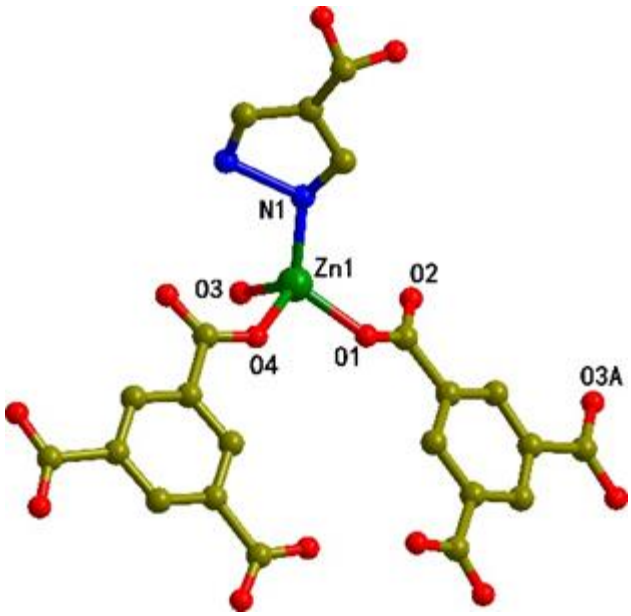

Fig. S1 The coordination environment of Zn(II) ion in NKU-**101**.

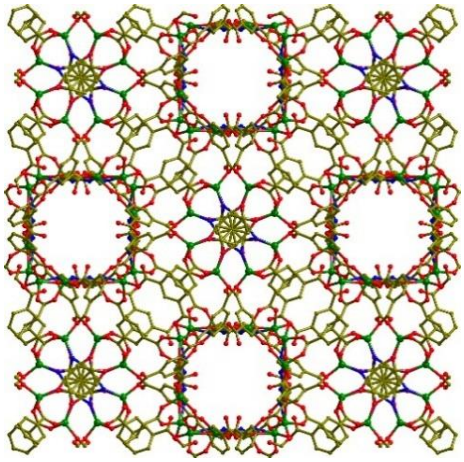

Fig. S2 The 3D structure of NKU-**101** intersected with cabined channels imbeded with uncoordinated O atoms on the wall. H atoms are omitted for clarity (similarly hereafter).

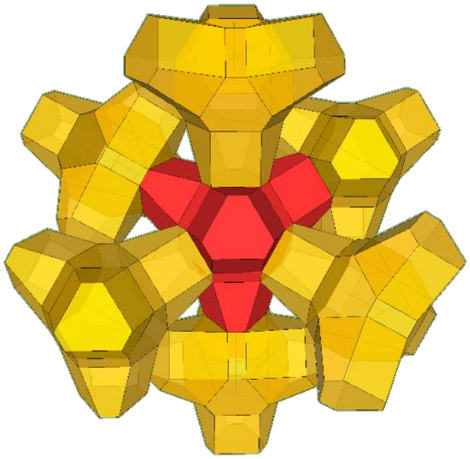

Fig. S3 The packing of tetrapodal cages in NKU-**101.**

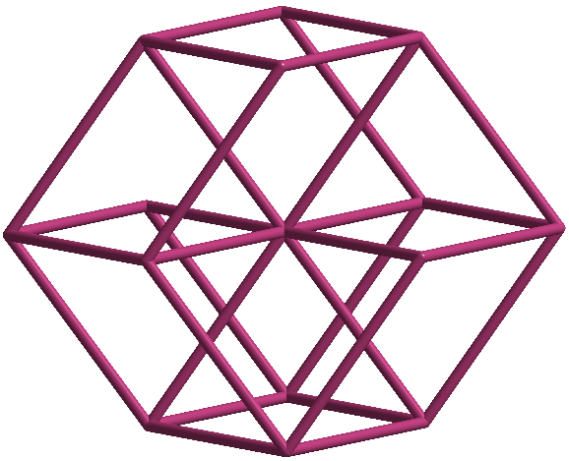

Fig. S4 The *bcu* network generated by considering the tetrapodal cage as a node.

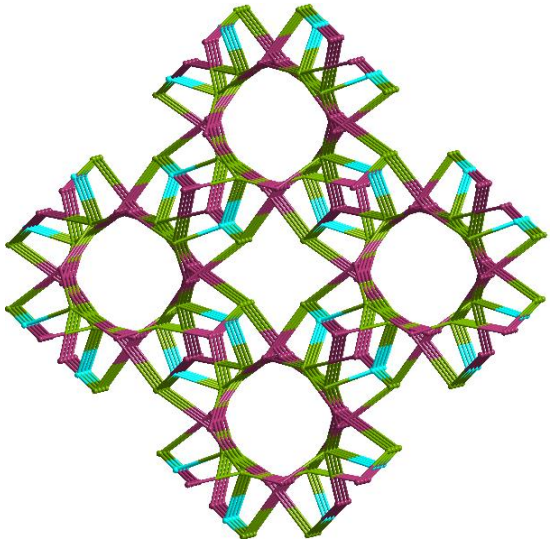

Fig. S5 The topologic structure of NKU-**101**.

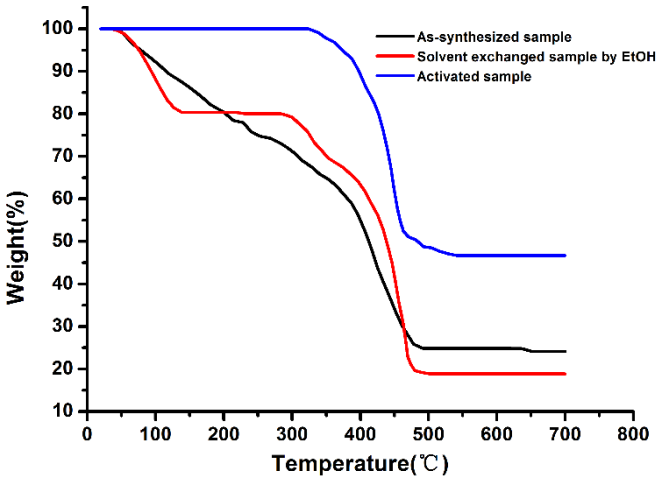

Fig. S6 The thermogravimetric curves of NKU-**101**.

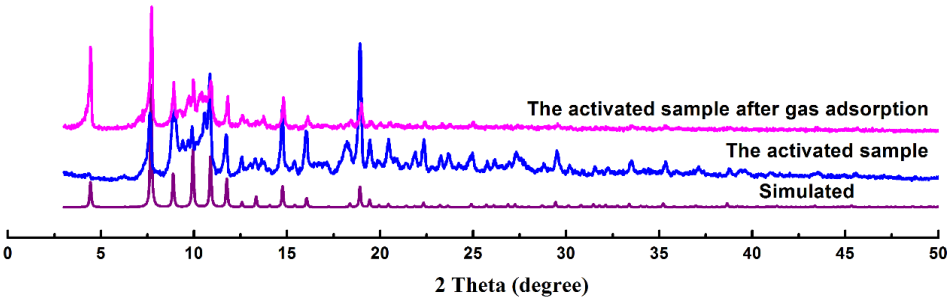

Fig. S7 The PXRD patterns of NKU-**101**: the simulated pattern based on X-ray single-crystal data (violet), the experimental pattern of activated sample (blue) and that after gas adsorption measurements (pink).

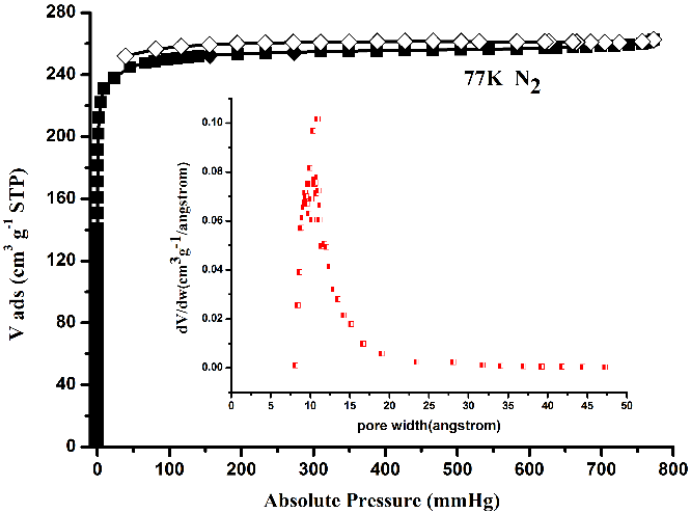

Fig. S8 N_2 sorption isotherms at 77 K. The filled and open symbols represent for the adsorption and desorption data, respectively. Inset: Horvath-Kawazoe pore size distribution plot of NKU-**101**.

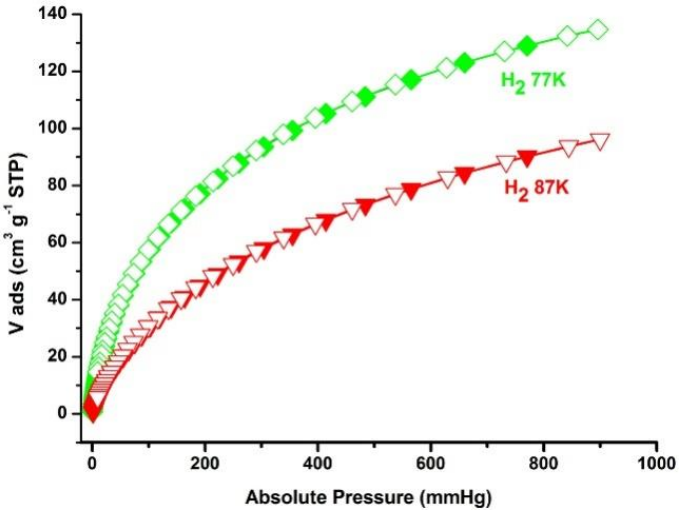

Fig. S9 H_2 Adsorption isotherms at 77 K and 87 K. The filled and open symbols represent for the adsorption and desorption data, respectively.

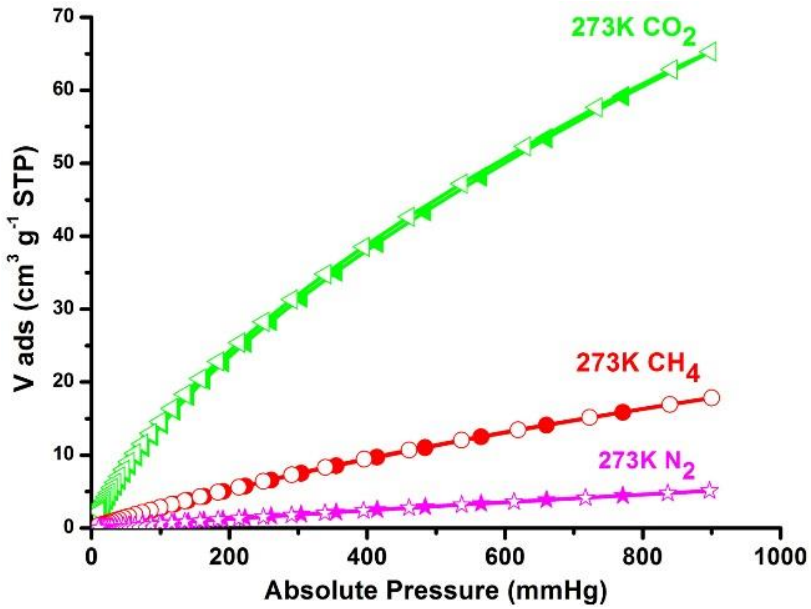

Fig. S10 The adsorption isotherms of CO_2, CH_4 and N_2 at 273 K. The filled and open symbols represent for the adsorption and desorption data, respectively.

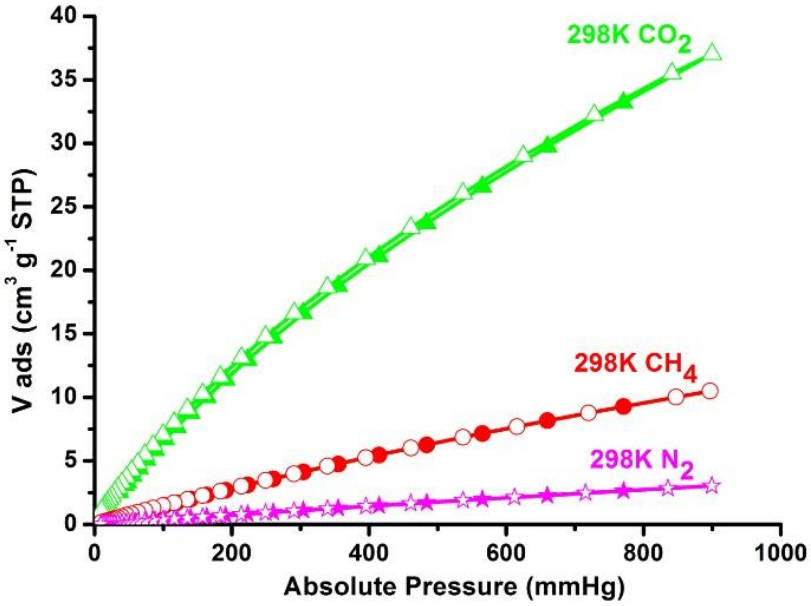

Fig. S11 The adsorption isotherms of CO_2, CH_4 and N_2 at 298 K. The filled and open symbols represent for the adsorption and desorption data, respectively.

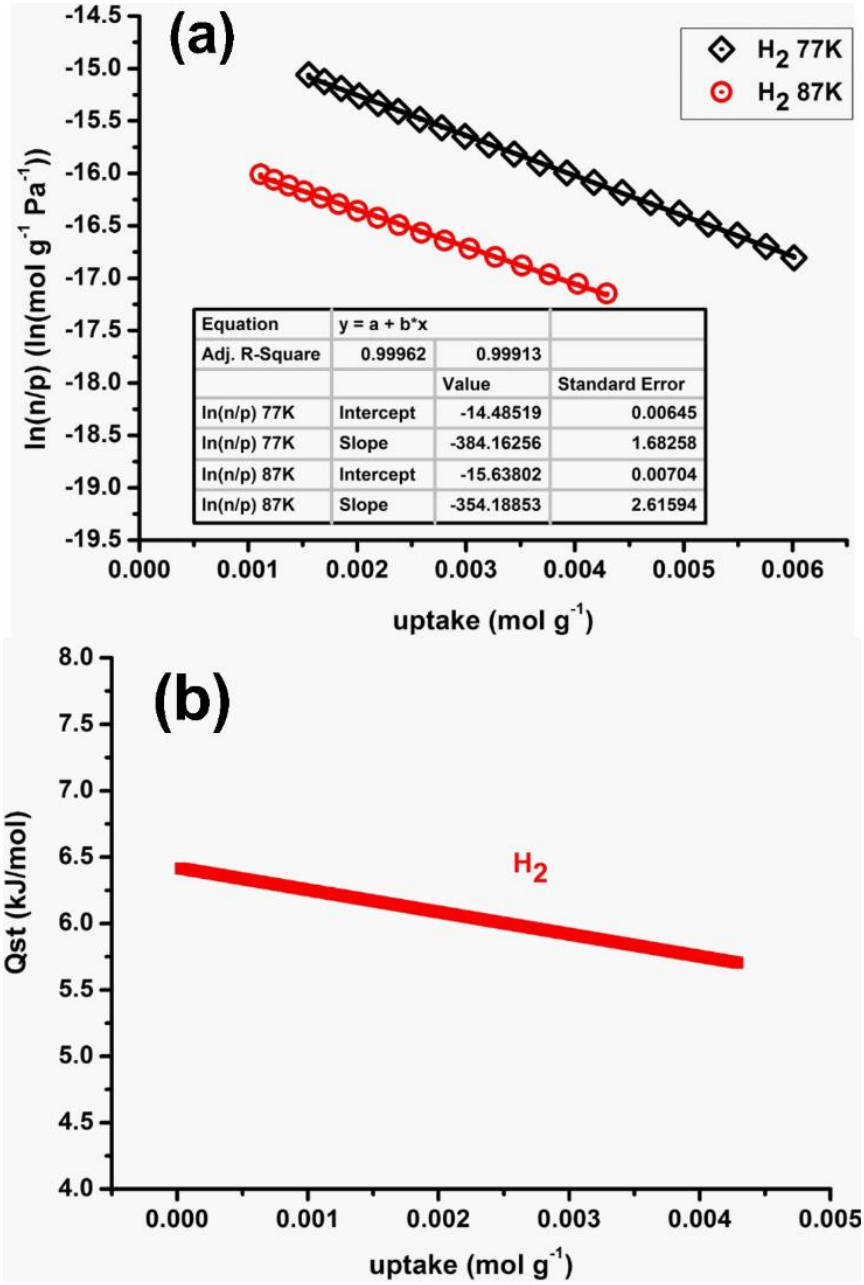

Fig. S12 The H_2 adsorption behaviors for NKU-**101.**[S3] (a) H_2 adsorption data fitted by Virial method and (b) H_2 adsorption enthalpy calculated by Virial method from the adsorption isotherms at 77 K and 87 K.

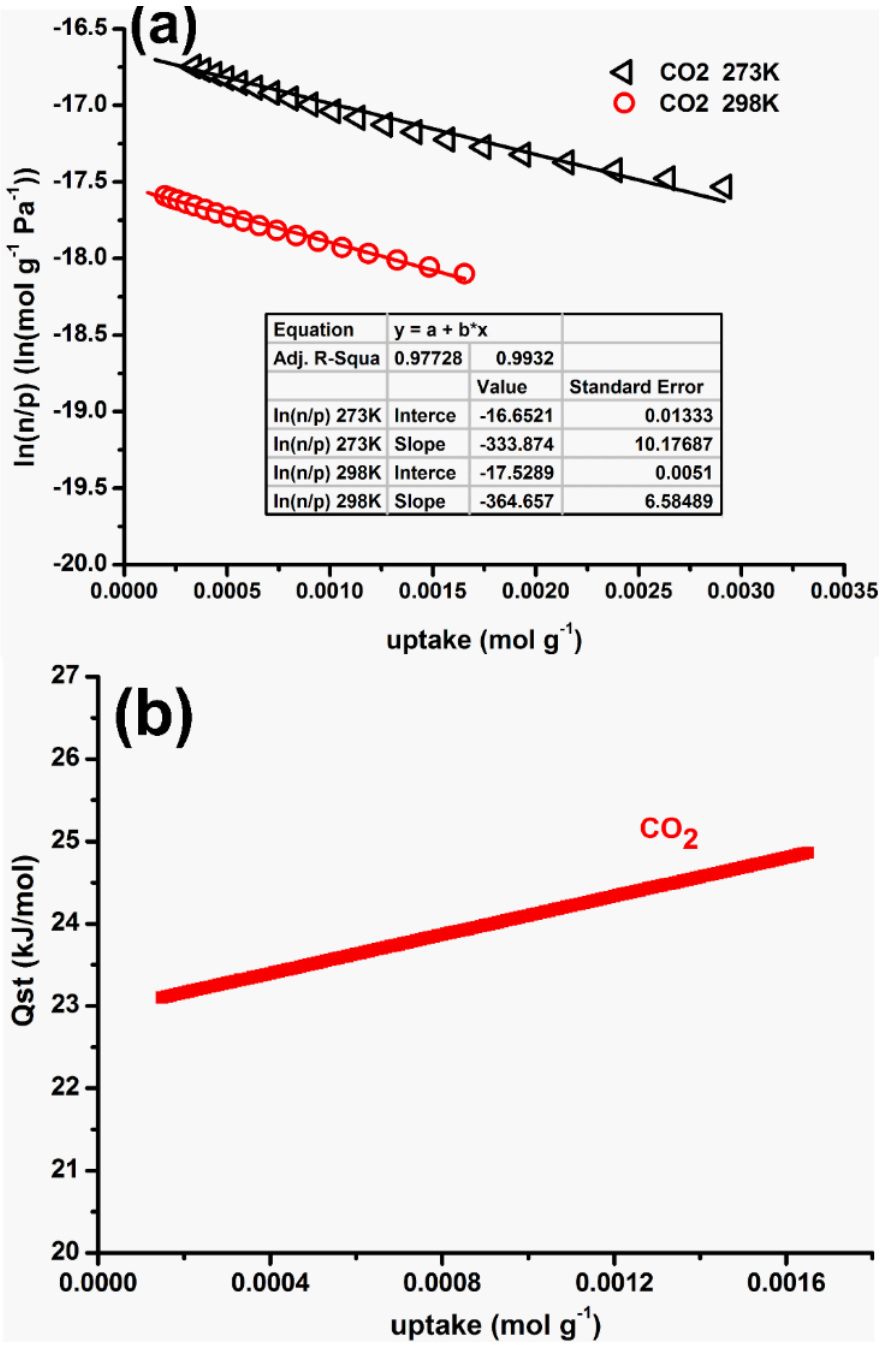

Fig. S13 The CO_2 adsorption behaviors**.** (a) CO_2 adsorption data fitted by Virial method and (b) CO_2 adsorption enthalpy calculated by Virial method from the adsorption data at 273 K and 298 K.

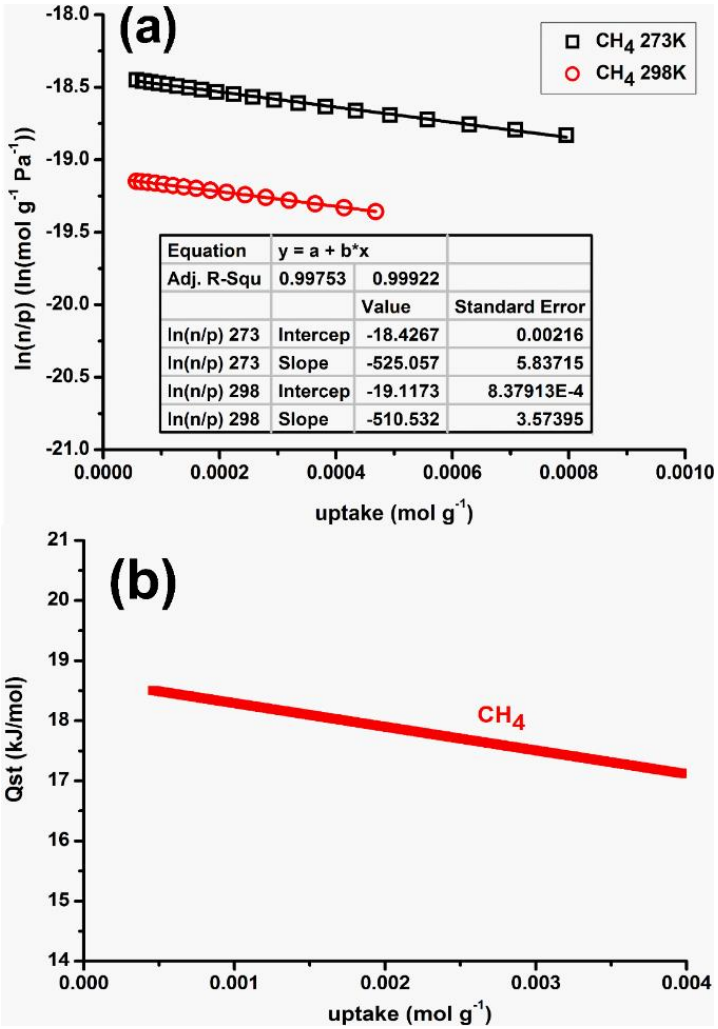

Fig. S14 The CH_4 adsorption behaviors**.** (a) CH_4 adsorption data fitted by Virial method and (b) CH_4 adsorption enthalpy calculated by Virial mehtod from the adsorption data at 273 K and 298 K.

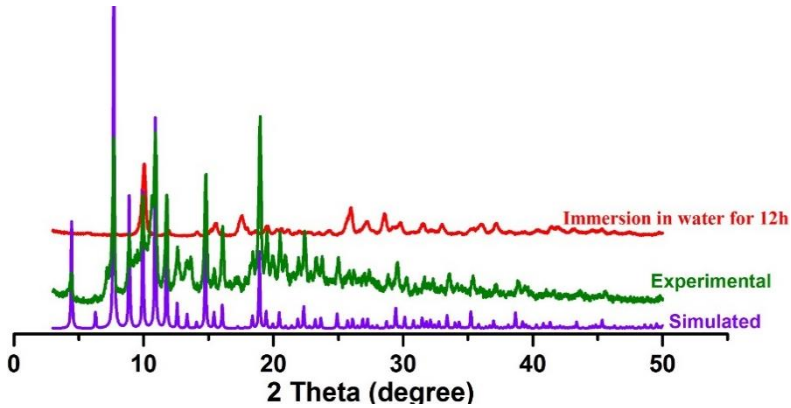

Fig. S15 The PXRD patterns of NKU-**101**: the simulated pattern based on X-ray single-crystal data (violet), the experimental pattern of activated sample (green) and that after immersion in water for 12 h (red).

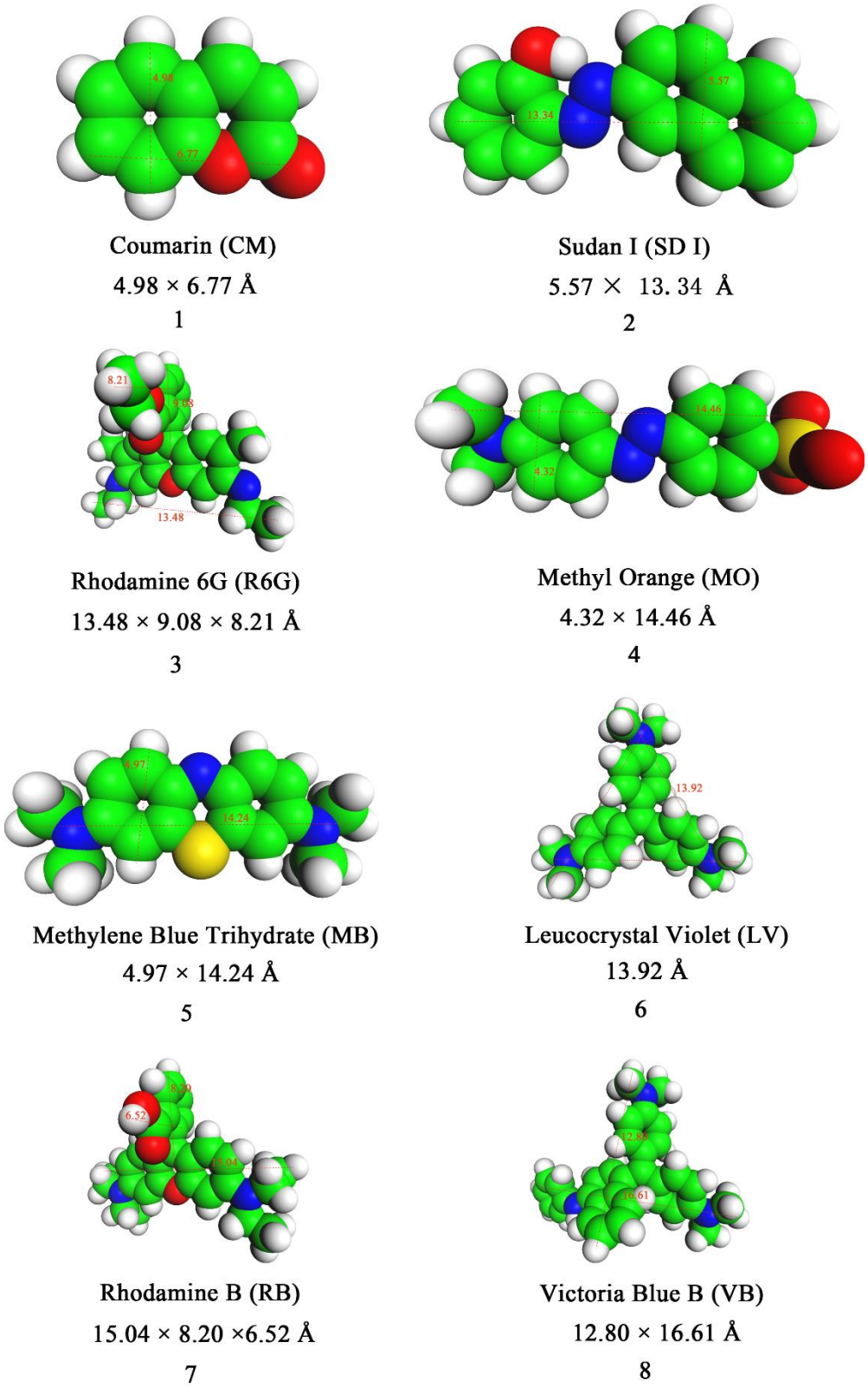

Fig. S16 The structures of eight dyes optimized by DFT calculation (in B3LYP/6-311G(d) level) with Gaussian 09 program package.[S4]

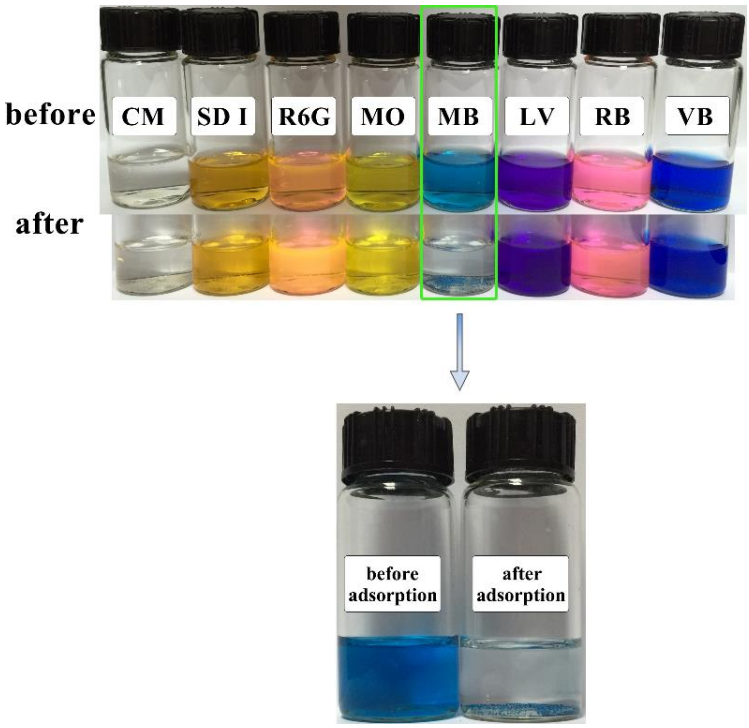

Fig. S17 Photographs of dye solutions before and after 24 h adsorption with NKU-**101.**

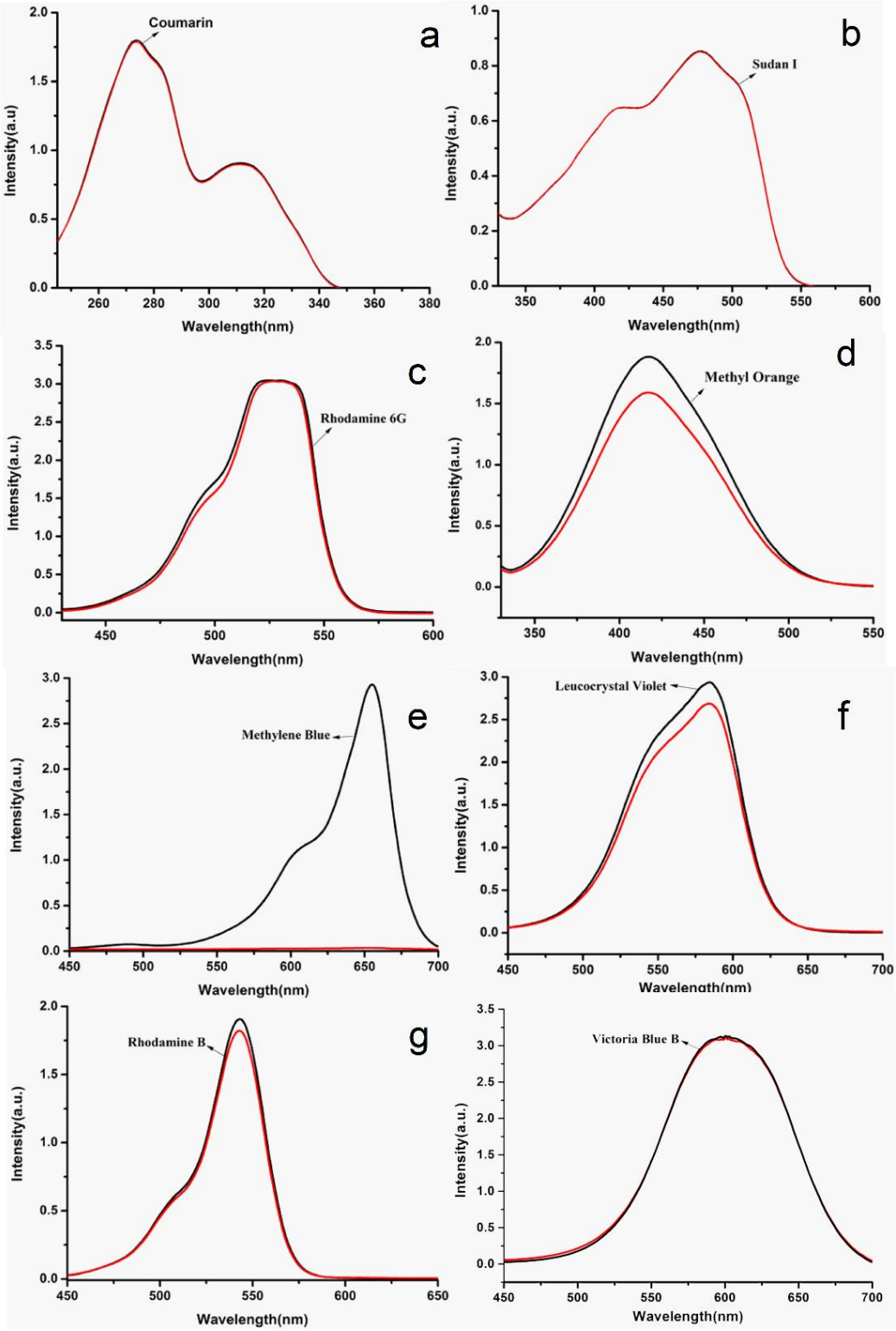

Fig. S18 UV/Vis absorption spectra of the EtOH solutions of dyes before (black) and after (red) 24 h adsorption with NKU-**101**.

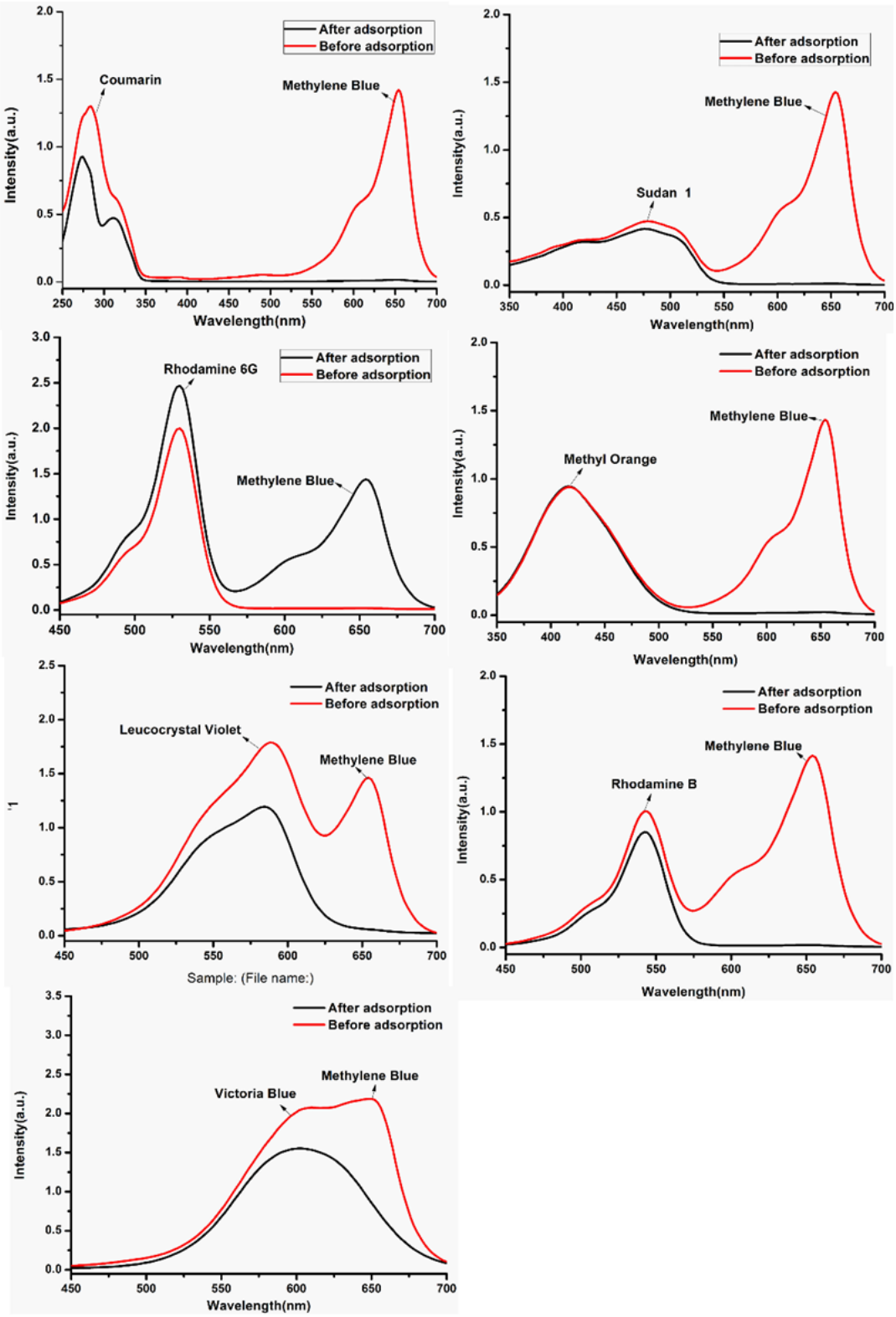

Fig. S19 UV/Vis absorption spectra of the EtOH solutions of mixed dyes before (red) and after (black) 24 h adsorption with NKU-**101**.

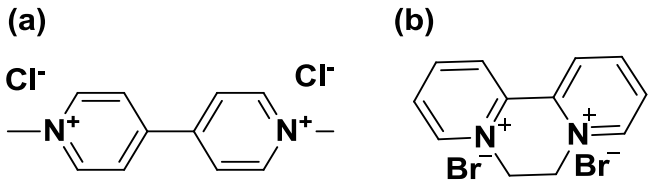

Fig. S20 The structures of (a) methyl viologen (b) and diquat.

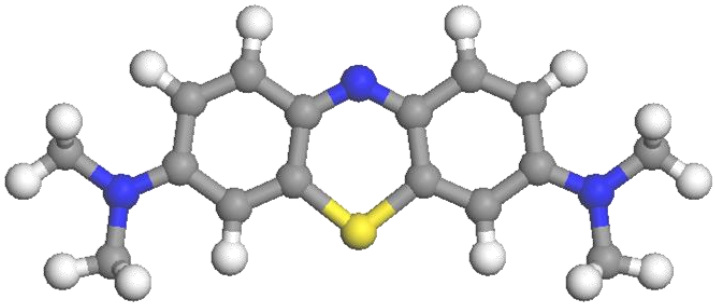

14.24×4.97Å

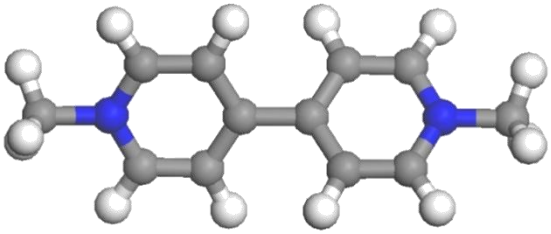

10.72×4.327Å

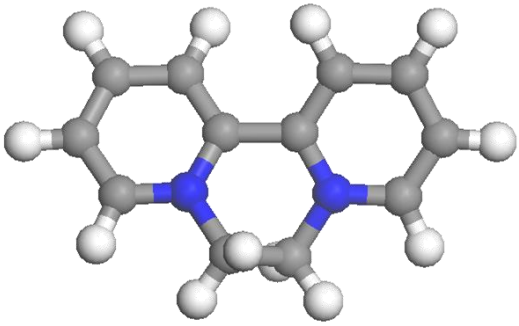

9.203×5.408Å

Fig. S21 The molecular structure optimized by DFT calculation (in B3LYP/6-311G(d) level) with Gaussian 09 program package.[S4] (a) methylene blue, (b) methyl viologen and (c) diquat.

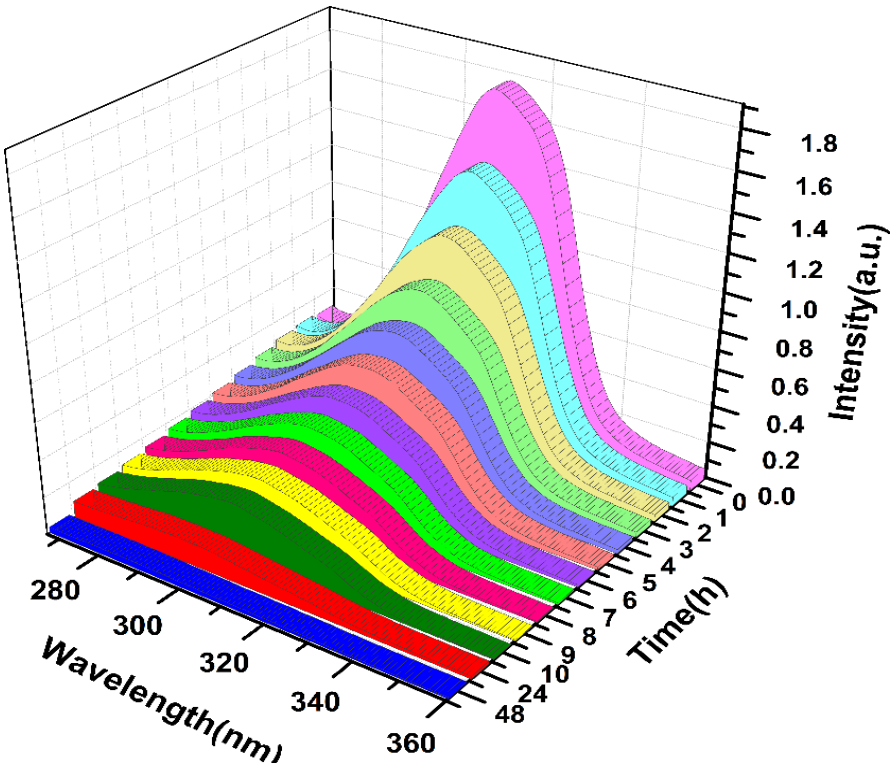

Fig. S22 Sequential change of the UV/Vis absorption spectra of DQ solution upon adsorpiton by NKU-**101**.

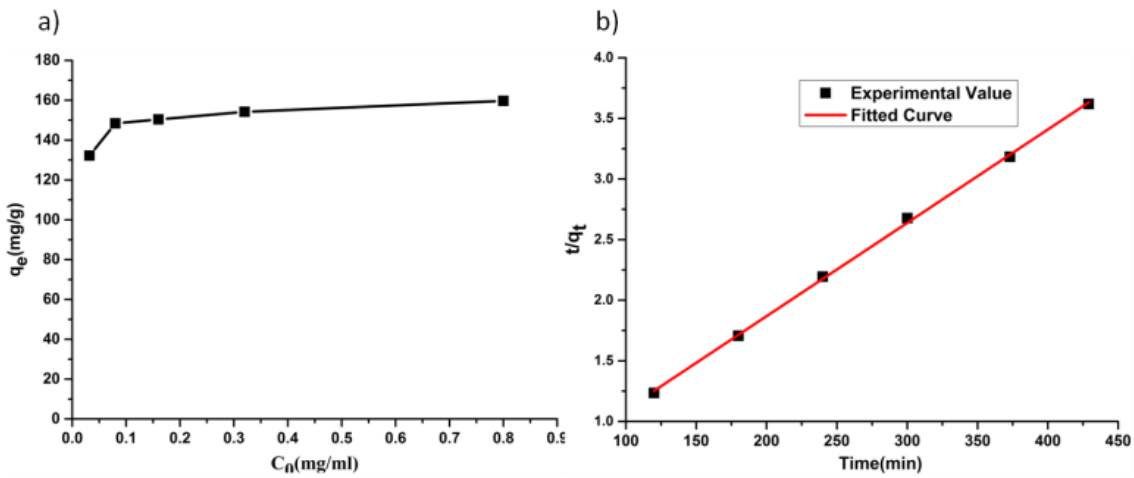

Fig. S23 The adsorption behaviours of MV by NKU-**101**. (a) The q_e-c_0 profile and (b) kinetic adsorption profile fitted by pseudo-second-order model.

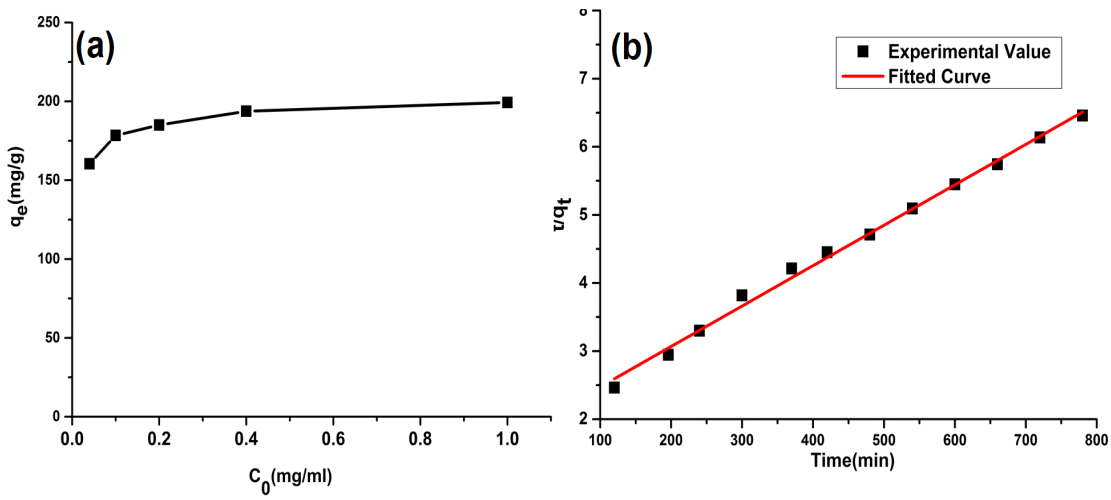

Fig. S24 The DQ adsorption behaviours of NKU-**101**. (a) The q_e-c_0 profile and (b) kinetic adsorption profile fitted by pseudo-second-order model.

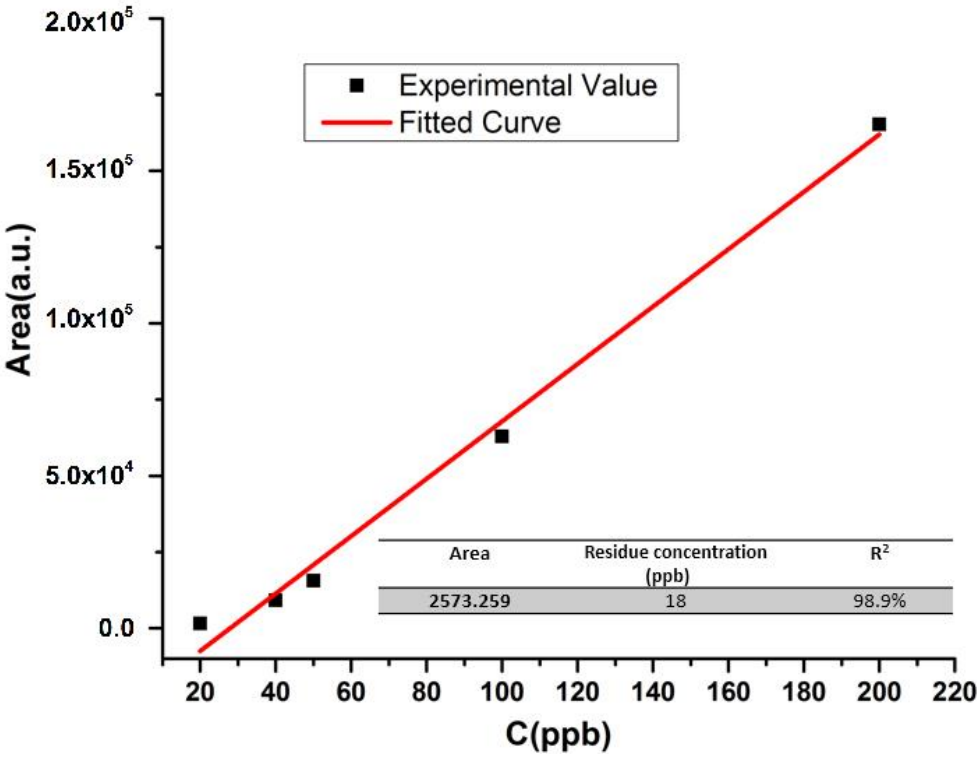

Fig. S25 The residues of MV upon adsorption by NKU-**101** in alcohol solution determined by LC-MS/MS. (The red curve is the standard concentration-peak areas of LC-MS/MS curve. The insert table shows the experimental datas of the residues of MV < 20 ppb.)

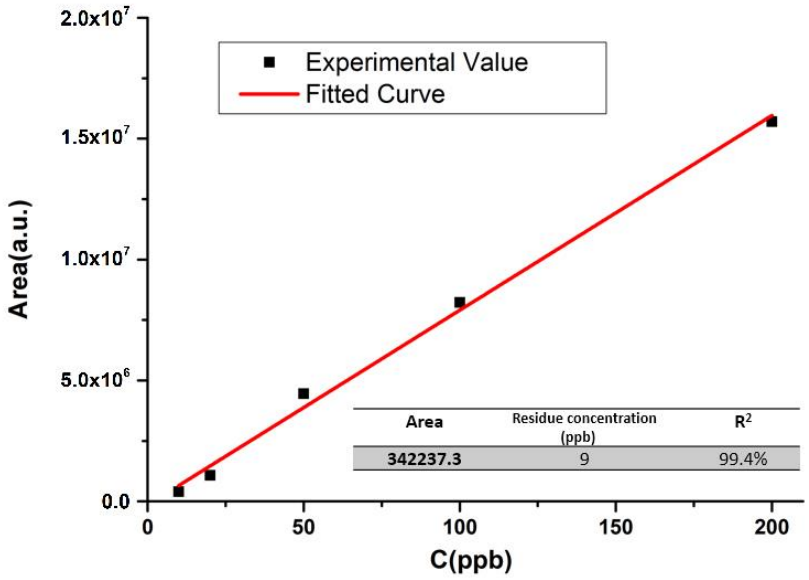

Fig. S26 The residues of DQ upon adsorption by NKU-**101** in alcohol solution determined by LC-MS/MS. (The red curve is the standard concentration-peak areas of LC-MS/MS curve. The insert table shows the experimental datas of the residues of DQ < 10 ppb.)

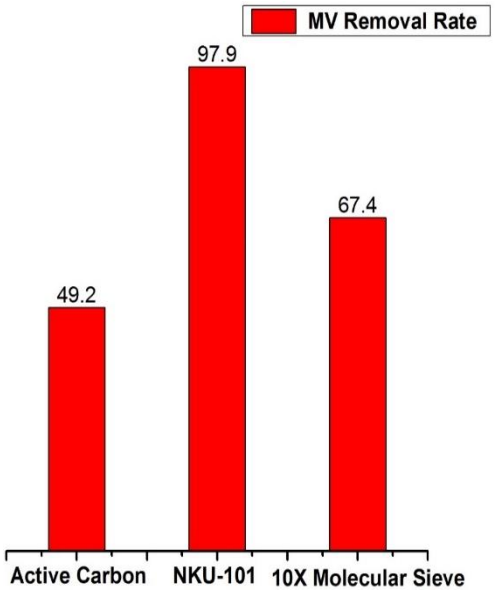

Fig. S27 The adsorption efficiency of active carbon, NKU-**101** and 10X molecular sieves in the removal of MV from ethanol for 48h (c_0 = 0.05 mg/ml).

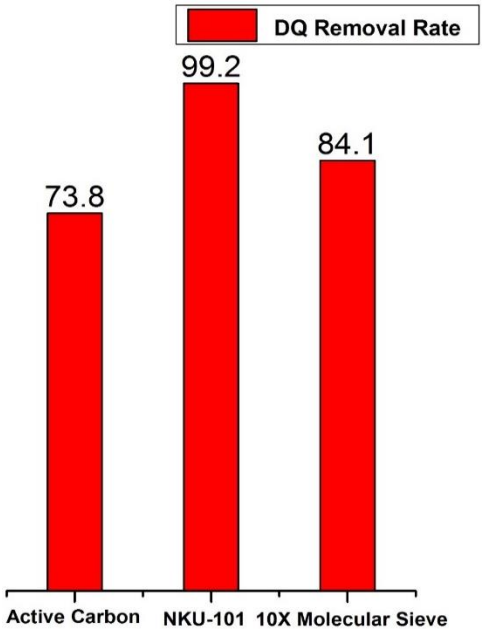

Fig. S28 The adsorption efficiency of active carbon, NKU-**101** and 10X molecular sieves in the removal of DQ from ethanol for 48h (c_0 = 0.05 mg/ml).

Table S1 The adsorption capacities of MV and DQ on avtivated carbon, NKU-**101** and 10X molecular sieves.

	Activated Carbon	10X Molecular Sieves	NKU-**101**
MV	70±5 mg	115±5 mg	160±5 mg
DQ	85±5 mg	130±5 mg	200±5 mg

The remove rate of MV and DQ is only 49.2 % and 73.8 % for activated carbon and 67.4 % and 84.1 % for 10X molecular sieve, respectively (Fig. S27 and S28), which is much smaller than the 97.9 % and 99.2 % for NKU-**101**. In addition, the adsorption capacities of MV and DQ by NKU-**101** are 2~3 times larger than that of activated carbon and 10X molecular sieve under the same condition (Table S1).

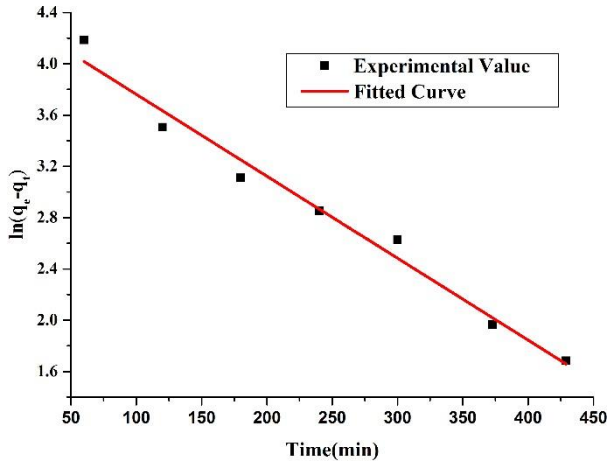

Fig. S29 The kinetic process of MV adsorption fitted with pseudo-first-order model.

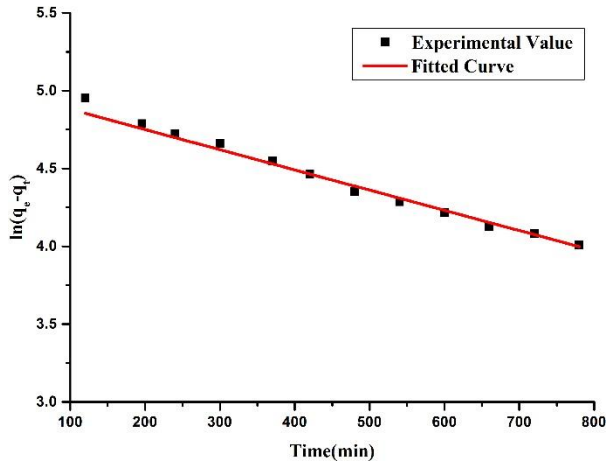

Fig. S30 The kinetic process of DQ adsorption fitted with pseudo-first-order model.

Table S2 Kinetic parameters for the adsorption of MV and DQ.

	q_e (Exp.) (mg/g)	pseudo-first-order model			pseudo-second-order model		
		k_1 (min^{-1})	R^2	q_e (Cal.) (mg/g)	k_2 $(mg/g)^{-1} \cdot min^{-1}$	R^2	q_e (Cal.) (mg/g)
MV	132	6.39×10^{-3}	97.6	81.6	1.81×10^{-4}	99.9	130
DQ	160	1.30×10^{-3}	98.4	150	1.87×10^{-5}	99.5	168

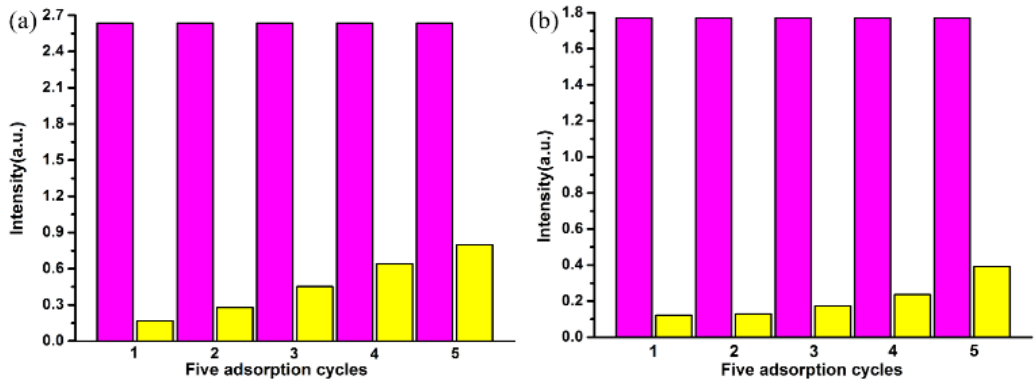

Fig. S31 The recyclic adsorption (24 h)-desorption (24 h) experiment presented by UV/Vis absorption intensity of (a) MV (262 nm) and (b) DQ (312 nm) in methanol solution (pink: before adsorption; yellow: after adsorption).

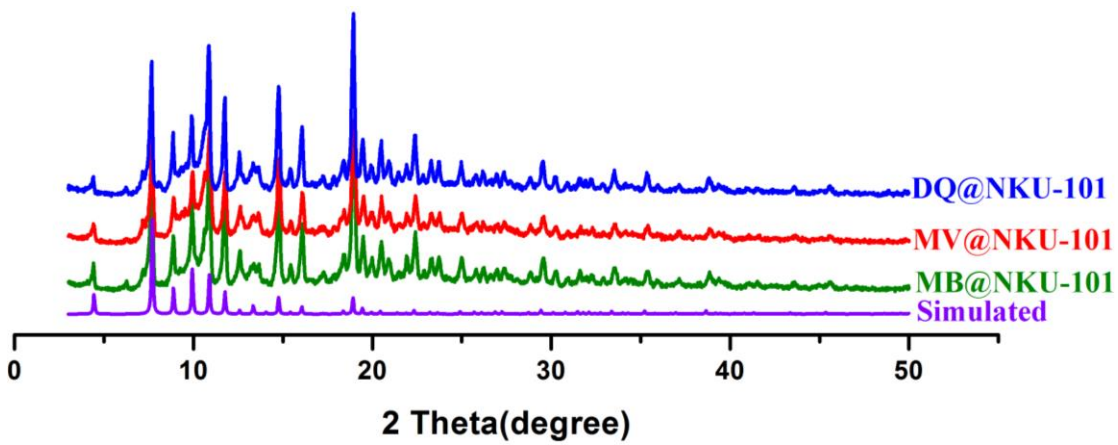

Fig. S32 The PXRD patterns of NKU-**101**: the simulated pattern based on X-ray single-crystal data (violet), the experimental pattern of NKU-**101** after MB adsorption (green), the experimental pattern of NKU-**101** after MV adsorption (red) and that after DQ adsorption (blue).

Eqs. S1

$$q_e = \frac{(c_0 - c_e)V}{m}$$

Where c_e, V, and m denote the equilibrium concentration of adsorbate, the volume of system and the mass of added adsorbent, respectively.

Eqs. S2a

$$\ln(q_e - q_t) = \ln q_e - \mathrm{k_1 t}$$

Eqs. S2b

$$\frac{t}{q_t} = \frac{1}{k_2 q_e^2} + \frac{t}{q_e}$$

Where q_t is the adsorption amount at time t, while k_1 ($\mathrm{min^{-1}}$) and k_2 ($(\mathrm{mg/g})^{-1}\cdot\mathrm{min}^{-1}$) denote the rate constants of the first-order and second-order adsorption process.

Table S3 The selected bond lengths [Å] and angles [º] of NKU-**101.**

Zn(1)-O(5)#1	1.887(14)
Zn(1)-O(1)	1.917(4)
Zn(1)-O(3)#2	1.950(4)
Zn(1)-O(4)	1.964(4)
Zn(1)-N(1)	1.981(15)

Symmetry transformations used to generate equivalent atoms:

#1 -x,y,-z+2; #2 y-1/2,-z+3/2,-x+3/2

Reference

[S1]. G. M. Sheldrick, SHELXL97, *Program for Crystal Structure Refinement*; University of Göttingen: Göttingen, Germany, 1997.

[S2]. A. L. Spek, *J. Appl. Crystallogr.*, 2003, **36**, 7.

[S3]. a) I. P. O'Koye, M. Benham, K. M. Thomas, *Langmuir*, 1997, **13**, 4054; b) C. R. Reid, I. P. O'Koy, K. M. Thomas, *Langmuir*, 1998, **14**, 2415; c) C. R. Reid, K. M. Thomas, *Langmuir*, 1999, **15**, 3206.

[S4]. *Gaussian 09, Revision B.01*: Frisch, M. J. et al.;. Gaussian, Inc.: Wallingford, CT, **2009**.